Synergizing Hardware and Software Energy Management for Reliable Start-Up and Operation of Battery-Free Electronic Devices

Jintao Meng, *Graduate Student Member, IEEE*, Jiacong Qiu, *Graduate Student Member, IEEE*, Yilin Wang, *Student Member, IEEE*, Minfan Fu, *Senior Member, IEEE*, Haoyu Wang, *Senior Member, IEEE*, and Junrui Liang, *Senior Member, IEEE*

***Abstract*—Advancements in Internet of Things (IoT) technologies have led to drastically increased demand for self-powered and sustainable electronic devices. Existing solutions for self-powered electronic devices typically use fixed-threshold undervoltage lockout (UVLO) circuits for energy buffering and release. The pure hardware design has some limitations. Small-scale energy storage systems often lack sufficient capacity to support large-scale software routines. On the other hand, large-scale energy storage systems undergo a prolonged start-up process. This delay occurs because the energy pool of large-scale systems needs to be filled up to the activation threshold before normal operation. In addition, a pure hardware-based UVLO lacks the capabilities of energy awareness and adaptivity. This article introduces a hardware–software collaborative energy management (EM) scheme and validates this EM scheme using a self-powered E-ink (SP-Eink) display. At the hardware level, an energy buffer-release (EBR) circuit is utilized. This circuit provides two hardware-defined on/off thresholds. At the software level, an adaptive EM (AEM) approach is designed. This approach achieves two software-tunable power-good and power-warning thresholds. The additional thresholds are created by polling the state of charge (SoC) through analog-to-digital converter (ADC) sampling. By leveraging the collaboration between the engineered hardware circuit and software routines, an SP-Eink node was developed. This node can not only achieve bidirectional information interaction with a computer host but also support a one-host-multiple-terminals working mode, making it widely applicable to the application requirements of multinode SP-Eink display scenarios. The proposed design offers valuable design references for low-cost, ultralow-power battery-free (BF) devices in ambient energy harvesting (EH) IoT systems.**

***Index Terms*—Adaptive energy management (AEM), battery-free (BF) Internet of Things (IoT) system, energy harvesting (EH), self-powered E-ink.**

I. Introduction

OVER the past few decades, the booming Internet of Things (IoT) has continuously promoted the in-depth integration of the cyber and physical worlds. Driven by the dual impetus of the global energy crisis and the "carbon neutrality" goal, self-powered electronic technologies have gradually expanded into diverse application scenarios. These technologies are characterized by a core advantage: capturing energy from the environment to realize autonomous power supply. Typical application scenarios of such technologies include smart homes and industrial monitoring [1], [2]. These self-powered systems utilize distributed ambient energy to construct low-power IoT terminals, which enable long-term autonomous operation [3], [4], [5]. However, the inherent volatility and spatial randomness of ambient energy have long restricted the performance stability of self-powered electronic devices. In particular, insufficient instantaneous energy supply tends to trigger operational interruptions of the system, while excessive energy may lead to problems including overload of storage modules and dissipation of energy efficiency [6], [7], [8]. Such contradictions make "energy supply-demand matching and sustainable system operation" a core challenge in the design of self-powered IoT devices [9], [10], [11], [12]. Fig. 1 illustrates the fundamental differences in energy management (EM) architectures and voltage waveforms between traditional battery-free (BF) energy harvesting (EH)-powered IoT devices and the proposed scheme in this article.

On the hardware layer, energy-sensing circuits exhibit inherent limitations [13]. These limitations include fixed threshold values, narrow hysteresis windows, insufficient energy-sensing capabilities, high static power consumption, and inadequate voltage resistance. These issues lead to delays in the cold start process of devices. They also pose challenges for adapting to dynamic variations in energy supply and demand. A variety of power management integrated circuits (ICs), voltage monitors/supervisors, and load switches have been developed, which provide optimized technical solutions for electrical EM [14]. However, EH-powered systems still encounter challenges in realizing adaptive, sustainable, and stable operation. Fig. 1(a) presents the EM architecture of traditional EH-IoT devices. This architecture adopts a classic combined topology of an undervoltage lockout (UVLO) circuit and a voltage regulator: the UVLO circuit performs real-time monitoring of the input voltage, and triggers a power cutoff mechanism when the voltage drops below the threshold UVLO to avoid device failure risks induced by low voltage [15], [16]; the

Received 1 July 2026; revised 3 August 2026; accepted 21 August 2026. Date of publication 25 August 2026; date of current version 9 November 2026. This work was supported by the National Natural Science Foundation of China under Grant 62271319. *(Corresponding author: Junrui Liang.)*

The authors are with the School of Information Science and Technology, ShanghaiTech University, Shanghai 201210, China, and also with Anhui Science and Technology University, Bengbu 233100, China (e-mail: mengjt2024@shanghaitech.edu.cn; qiujc@shanghaitech.edu.cn; wangyl22002@shanghaitech.edu.cn; fumf@shanghaitech.edu.cn; wanghy@shanghaitech.edu.cn; liangjr@shanghaitech.edu.cn).

Digital Object Identifier 10.1109/JIOT.2026.3727271

2327-4662 © 2026 IEEE. All rights reserved, including rights for text and data mining, and training of artificial intelligence and similar technologies. Personal use is permitted, but republication/redistribution requires IEEE permission.
See https://www.ieee.org/publications/rights/index.html for more information.
Authorized licensed use limited to: ShanghaiTech University. Downloaded on November 09,2026 at 03:10:32 UTC from IEEE Xplore. Restrictions apply.

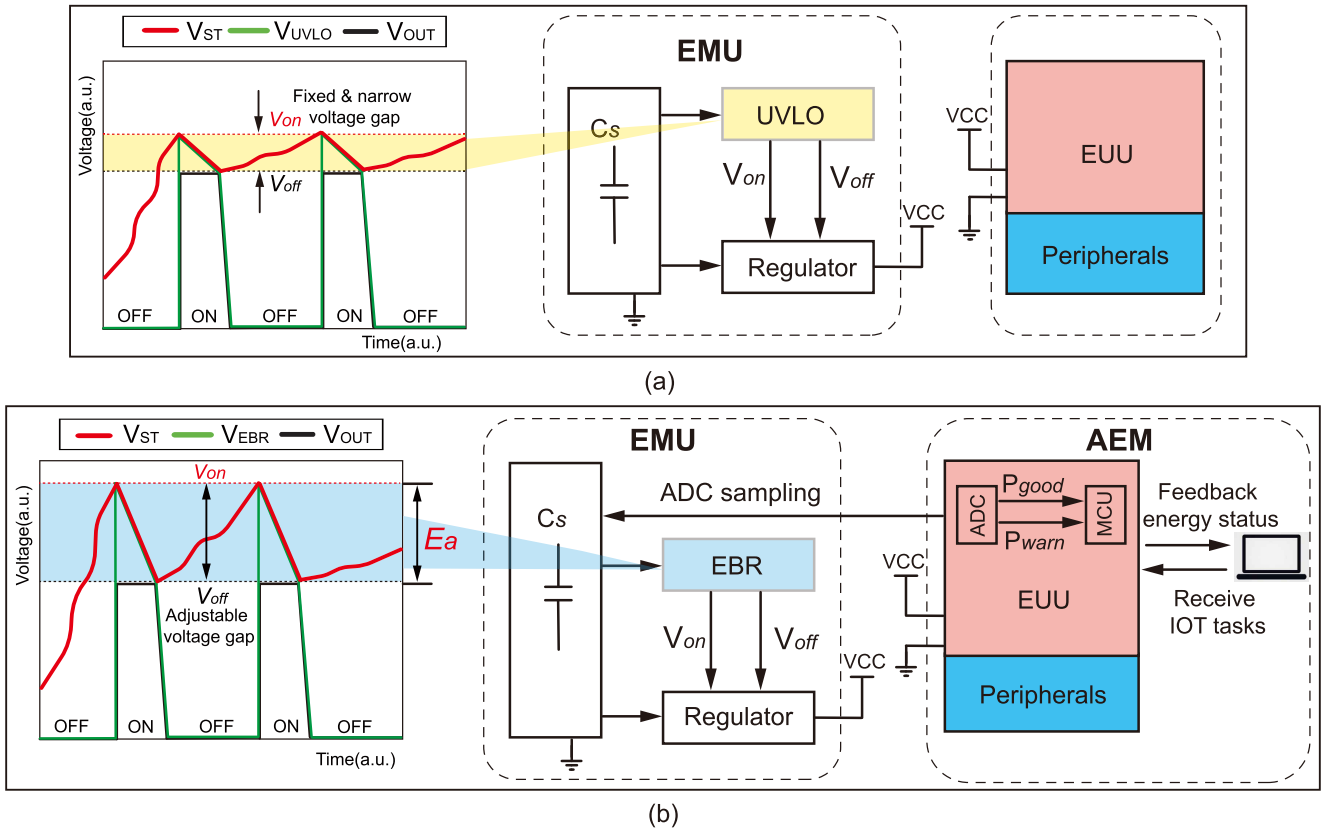


Fig. 1. Schematics of power supply solutions for a self-powered IoT device. (a) Hardware UVLO for EM. (b) Hardware–software collaborative EM.

voltage regulator is responsible for ripple filtering and stable power output [17], [18]. In addition, the narrow hysteresis voltage window between the turn-on threshold V_{on} and the turn-off threshold V_{off} fundamentally limits the dynamic range of energy regulation [19], [20]. To meet the energy buffering requirement, a large-capacity energy buffer capacitor is often required, which not only increases the hardware volume and cost but also restricts the system integration [21]. Fig. 1(b) shows the innovative EM architecture of EH-IoT proposed in this article. Based on the traditional architecture [22], a reconfigurable energy buffer-release (EBR) circuit is introduced to achieve breakthrough improvements: after the EH energy is intermittently accumulated in the storage element through the interface circuit, the start-stop control of the load is completed by monitoring the storage voltage V_{ST} (the load is activated when the voltage reaches V_{on}, and the power supply is turned off when the voltage is lower than V_{off}). Compared with the traditional architecture, this scheme realizes the continuous adjustability of the threshold interval between V_{on} and V_{off} through a resistor network, eliminates the narrow hysteresis window constraint of the traditional UVLO circuit, thereby avoiding the dependence on large-capacity energy buffer capacitors [23], and significantly improves the flexibility of energy regulation and the energy utilization efficiency of the system [11], [24]. By fine-tuning the switching threshold voltage difference and selecting a capacitor with an appropriate capacitance value, the required energy is matched with the supplied energy to achieve a balance between supply and demand, which is crucial for BF IoT systems [25], [26].

On the software layer, EM strategies (e.g., prescheduled operating modes, dynamic operating mode switching) generally lack hardware adaptability and power-adaptive mechanisms. These strategies perform scheduling independently of the actual energy status of the hardware, which readily causes frequent system wake-ups or operational interruptions under energy fluctuations, leading to inadequate scenario adaptability [27]. In addition, the cold-start voltage threshold of traditional UVLO circuits exhibits a strong correlation with the state of charge (SoC) of energy storage components. If the cold-start threshold is not decoupled from the SoC indication threshold, an additional energy accumulation phase cannot be realized. Traditional UVLO circuits also lack the capability of SoC feedback [28], [29]. Pure hardware-based UVLO designs possess inherent limitations: Small-capacity energy storage systems are unable to support the operation of large-scale software routines, while large-capacity energy storage systems require charging the energy pool to the activation threshold for proper functionality, leading to long start-up delays and the lack of energy sensing and adaptive capabilities [30], [31], [32].

To address the above issues, this article proposes a hardware–software collaborative EM scheme. The primary objective of the proposed scheme is to enhance the collaborative performance between hardware and software components

Authorized licensed use limited to: ShanghaiTech University. Downloaded on November 09,2026 at 03:10:32 UTC from IEEE Xplore. Restrictions apply.

in EM. It also aims to ensure the stable operation of self-powered IoT devices. At the hardware layer, the proposed scheme employs an EBR circuit to implement two hardware-defined on/off thresholds. Notably, it exhibits two key features: reconfigurable voltage thresholds and enhanced voltage hysteresis. At the software layer, this article proposes an adaptive EM (AEM) method. This method sets two software-adjustable power-good thresholds and power-warning thresholds. These additional thresholds are generated by polling the SoC of the battery through analog-to-digital converter (ADC) conversion sampling, providing supplementary support for the EBR circuit. The two extra software-defined thresholds can be dynamically adjusted according to the operating conditions of the cyclically running programs, enabling adaptive energy budget allocation and ensuring the stable execution of IoT tasks with different energy consumption requirements. This article uses the information interaction between SP-Eink and the host computer as a verification platform to implement the proposed hardware–software collaborative EM scheme. The developed SP-Eink node enables bidirectional information interaction with a computer host. It supports the host-multiple-terminal operating mode. This node can be widely applied to meet the application requirements of multinode self-powered electronic ink screen displays. The proposed design offers valuable design references for BF devices in ambient EH IoT systems.

II. Related Works

This section focuses on the collaborative EM of hardware and software to achieve the reliable start-up and operation of batteryless electronic devices. It reviews relevant research on energy release mechanisms in the field, categorizes existing studies into two major directions: 1) research on energy-aware circuits and 2) software-layer EM strategy research.

A. Research on Energy-Aware Circuits

In a typical energy-harvesting IoT system module, the EM unit (EMU) serves as a core component. However, most existing studies on EMUs fail to sufficiently emphasize the design of the EBR circuit, which is a key part of the overall EM scheme. Currently, EM schemes based on hardware circuits are mainly classified into three categories. Each type of scheme exhibits significant defects in practical engineering applications. The specific analysis is presented as follows.

1) UVLO-Integrated EH ICs: Some EH application-specific ICs have a built-in UVLO function. A typical example is the LTC3588 from Analog Devices, which is tailored for piezoelectric EH scenarios. The UVLO hysteresis threshold of such chips is a fixed value, with a threshold gap ranging approximately from 1 to 1.38 V. The available energy for intermittent operation can only be adjusted by modifying the capacitance of the energy buffer capacitor. The insufficient voltage gap of the UVLO hysteresis imposes constraints on the available energy. To satisfy the energy requirements of IoT nodes for completing a single task, an energy buffer capacitor with a larger capacitance must be employed.

2) Universal Voltage Supervisors: For EH scenarios, standalone UVLO chips have been specifically designed, such as the TPS3839 and TPS3840 models manufactured by Texas Instruments (TIs). These chips are typically employed to detect the storage voltage of EH systems and control the operation of EH circuits [33]. A core drawback of these standalone UVLO chips lies in their fixed threshold voltage and an extremely narrow hysteresis window, where the window width is usually less than 300 mV. This characteristic leads to a low level of available operating energy for IoT nodes that rely on EH systems. Under low-voltage conditions (e.g., supply voltages below 1 V), the performance of these UVLO chips becomes unstable. In particular, the transistors inside the chip enter a subthreshold region, which induces uncertain output signals and unnecessary leakage currents. As a result, these standalone UVLO chips cannot be directly applied to circuits that require start-up from a 0 V initial voltage.

3) Dual Voltage Detectors: Essentially, these devices function as comparators integrated with an internal voltage reference. Their turn-on (V_{on}) and turn-off (V_{off}) thresholds can be adjusted through external resistors. Representative commercial products include the MIC841 manufactured by Microchip and the TPS3806 produced by TIs. The quiescent current of these devices is relatively high, with 1.5 μA for the MIC841 and 3 μA for the TPS3806. This level of quiescent current fails to meet the ultralow power consumption requirements of EH applications [34]. In addition, their maximum withstand voltages are relatively low, being 5.5 and 7 V, respectively. This low maximum withstand voltage makes it challenging to satisfy the high input voltage requirements (tens to even hundreds of volts) in specific EH scenarios, such as piezoelectric and triboelectric EH [35].

In summary, the three aforementioned hardware circuit-based EM schemes exhibit multiple drawbacks in practical engineering applications. To address the design challenges and requirements of EM IoT devices, this article proposes a novel EM circuit. This circuit features four core characteristics: energy sensing capability, ultralow power consumption, reduced component count, and adjustable start-up/shutdown voltage thresholds. The specific design principles, parameter selection criteria, and performance verification methods are elaborated in detail in Section III of this article.

B. Software-Layer EM Strategy Research

The EM algorithm serves as a core technology for the operation of IoT devices. It can dynamically adjust power allocation and the working modes of components according to the device's energy status, task requirements, and energy supply conditions. On the premise of ensuring the complete implementation of system functions, this algorithm is capable of minimizing energy consumption. Such minimization of energy consumption enables effective extension of the device's battery life and significant improvement in energy utilization efficiency. Currently, EM algorithms can be divided into the following two major categories.

1) Prescheduled Operating Mode: The core advantage of the proposed strategy lies in its capability to dynamically switch the operating mode of a device based on the

Authorized licensed use limited to: ShanghaiTech University. Downloaded on November 09,2026 at 03:10:32 UTC from IEEE Xplore. Restrictions apply.

TABLE I
COMPARISON BETWEEN EXISTING EM TECHNOLOGIES AND THIS WORK

Literature	Battery-free	Energy feedback	Real-time	Low power	Cold start reduction	intermittent	Prototyped
D. Lin et al. [36]	√	√	—	√	—	√	—
DoSR [37]	—	—	—	—	—	—	—
DPA & RIM [38]	—	—	√	√	—	—	—
Wang et al. [39]	√	—	√	√	—	√	√
MOEA/D [40]	—	—	√	√	—	—	—
TS [41]	—	—	√	—	—	—	—
DPM [42]	—	—	√	√	—	—	√
G. Loubet et al. [43]	√	—	√	√	—	√	√
Qiu et al. [44]	√	—	√	√	—	√	—
Zhu et al. [45]	√	—	√	√	—	√	—
DEAS et al. [46]	√	—	√	√	—	√	—
Kim et al. [47]	√	—	√	—	—	√	√
Huang et al. [48]	—	√	√	—	—	—	√
Chen et al. [25]	√	—	√	√	—	√	√
This work	√	√	√	√	√	√	√

"fluctuation-stability" characteristics of monitoring parameters (e.g., pressure and temperature) [49]. This capability enables real-time responses to parameter anomalies, eliminates ineffective energy consumption, and adapts to the actual operational requirements of relevant scenarios. However, this strategy exhibits inherent limitations, which are summarized as follows. First, its hardware adaptability is insufficient: it fails to perform targeted optimization for similar core components (e.g., low-power sensors and converters), thereby restricting the energy consumption control effect under low-voltage operating conditions. Second, it lacks a power adaptive regulation mechanism; this mechanism is absent because the remaining energy status of the device is not fully considered. The absence of such a mechanism makes the system susceptible to functional anomalies or disruptions induced by "excessive wake-ups" when the energy supply is insufficient [50], [51].

2) Dynamically Switch Working Mode: The core advantage of this proposed strategy lies in its ability to plan the operating mode of the device based on predefined task cycles. This planning approach reduces the start-stop losses induced by the temporary switching of functional modules. Meanwhile, it ensures that the device maintains a stable and active state during the execution of critical tasks [51]. However, this strategy exhibits a limitation of insufficient scenario adaptability. In particular, the fixed predefined cycles make it challenging to cope with dynamic changes, such as sudden mutations in environmental parameters. In addition, this strategy lacks a scenario-differentiated design. It fails to perform customized optimization for different energy output conditions. As a result, the overall energy utilization efficiency is limited in various scenarios with unstable energy supply [52].

Table I compares the AEM strategy proposed in this article with existing EM technologies reported in the current literature. All the aforementioned research works focus on application fields associated with EH and EM. However, the EM technology schemes in the existing literature exhibit significant limitations.

1) *Hardware Limitations:* Pure hardware-based UVLO circuits adopt fixed threshold levels and narrow hysteresis windows, which prohibit the configuration of adjustable energy windows.
2) *Software Limitations:* Traditional software-based EM overrelies on predefined fixed sleep cycles and static scheduling strategies. This overreliance results in frequent cold starts, considerable unnecessary energy consumption, and nonnegligible latency.
3) The lack of real-time sensing of the underlying hardware energy status leads to poor adaptability. It also causes difficulty in meeting diverse IoT task requirements.

To address the aforementioned issues, this article proposes an AEM method. The AEM method acquires the SoC via ADC sampling. Two software-adjustable power thresholds are configured to provide supplementary support for the EBR circuit. These thresholds can be dynamically adjusted according to the operating state of the program. This adjustment enables adaptive allocation of energy budgets. It ensures stable execution of IoT tasks with different energy consumption levels. Meanwhile, the AEM method completes feedback on the device's energy status and fault monitoring. The specific design of the AEM method is detailed in Section III.

III. SYSTEM OVERVIEW

Fig. 2 shows the system architecture of the hardware–software collaborative EM scheme designed for the light-powered E-ink display. It consists of five key components.

1) Energy source and storage module for converting ambient light energy into electrical energy and storing this energy in a small capacitor, as shown in Fig. 2(a).
2) EBR circuit, as shown in Fig. 2(b), for ensuring near-zero leakage when shunted down and a rapid release when sufficient energy is accumulated.
3) Microcontroller Unit (MCU) and ADC for executing the IoT tasks, as shown in Fig. 2(c).
4) The E-ink peripheral module, as shown in Fig. 2(d), for providing a display to the user according to the received information from a host device.
5) AEM software routine, as illustrated in Fig. 2(e), for in-program adjustment by adapting to different load energy demands.

Authorized licensed use limited to: ShanghaiTech University. Downloaded on November 09,2026 at 03:10:32 UTC from IEEE Xplore. Restrictions apply.

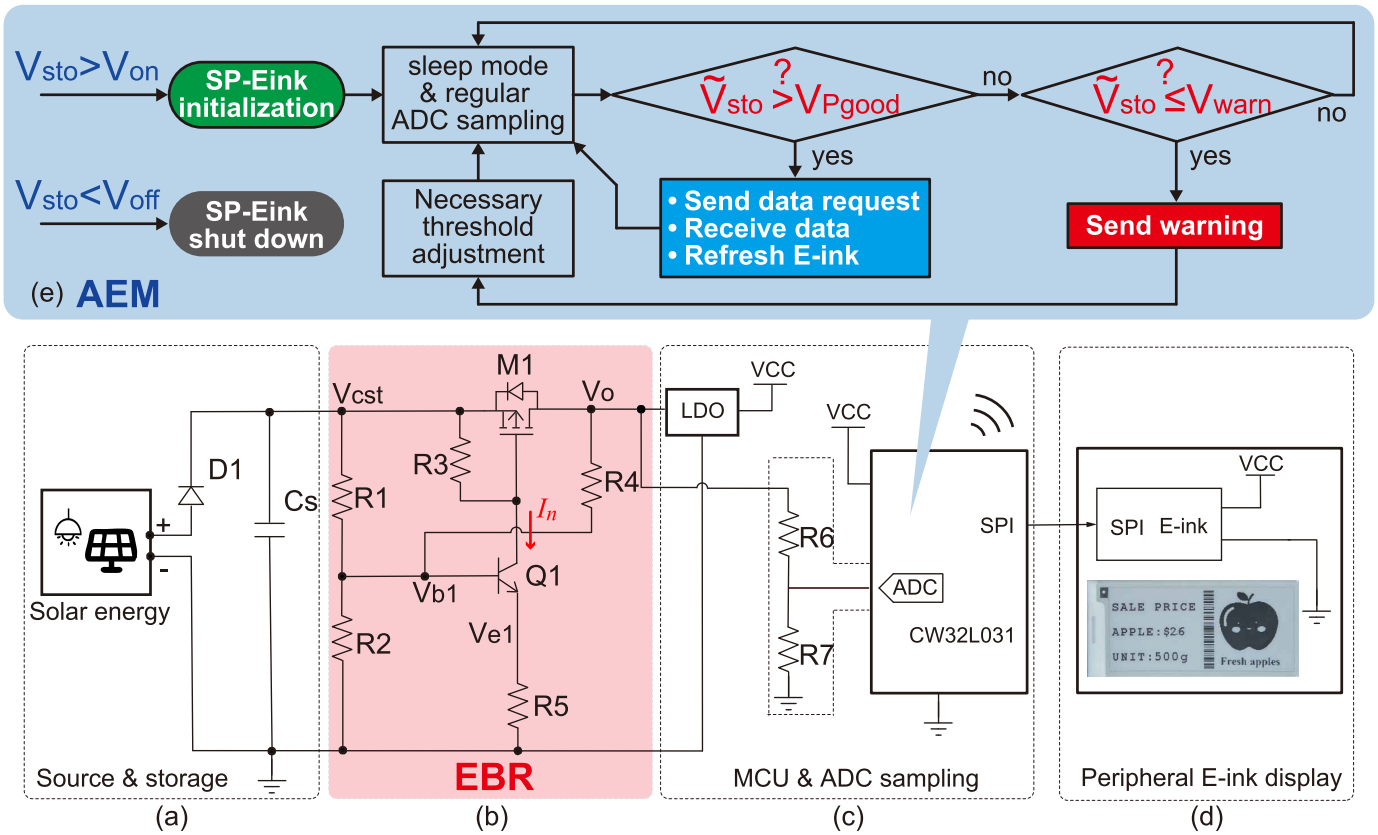


Fig. 2. System configuration of the hardware EBR and software AEM collaborative EM. (a) Source and storage. (b) EBR circuit. (c) LDO and MCU. (d) Peripheral. (e) AEM scheme.

A. Hardware EM Using EBR

Although EBR shares the same core functionality as the conventional UVLO circuit module, critical design differences still exist between them. In particular, the hysteresis window of EBR can be adjusted through a resistor network. For controlling the specific amount of energy released from a small storage, the voltage hysteresis between V_{on} and V_{off}, i.e., turn-on and turn-off thresholds, must be more significant in the EBR case.

1) Theoretical Derivation of the EBR Circuit: As shown in Fig. 2(b), the turn-on threshold V_{on} can be calculated as the value of V_{cst} when v_{R3}, the voltage across R_3, reaches the threshold voltage of the MOSFET M_1. The critical value of the current I_n, also the collector current through Q_1, can be formulated as follows:

$$I_{n,\text{cr}} = |V_{\text{th},p}|/R_3 \tag{1}$$

where $V_{\text{th},p}$ is the threshold voltage of M_1. The base–emitter voltage difference of Q_1 is given as follows:

$$V_{\text{be1,cr}} = V_{\text{T}} \ln\left(I_{n,\text{cr}}/I_{\text{s}}\right) \tag{2}$$

where V_{T} is the thermal voltage, around 25.9 mV at room temperature. I_{s} is the constant saturation current of Q_1. It can be extracted from the relationship between the base–emitter voltage and the collector current in the data sheet. Given that the collector current is approximately equal to the emitter current for a large-gain bipolar junction transistor, the emitter voltage

$$V_{\text{e1,cr}} \approx I_{n,\text{cr}} R_5. \tag{3}$$

When M_1 is off, $V_o = 0$. The relationship between V_{on} and $V_{b1,cr}$ can be formulated as follows:

$$V_{\text{on}} = \frac{R_1 + R_2 \parallel R_4}{R_2 \parallel R_4} V_{\text{b1,cr}} \tag{4}$$

where "$\parallel$" denotes the parallel connecting relation. Substituting (2) and (3) into (4), the turn-on threshold is formulated as follows:

$$V_{\text{on}} = \frac{R_1R_2 + R_1R_4 + R_2R_4}{R_2R_4}\left[I_{n,\text{cr}}R_5 + V_T \ln\left(\frac{I_{n,\text{cr}}}{I_s}\right)\right]. \tag{5}$$

After M_1 conducts, $V_o = V_{cst}$. R_4 is connected in parallel with R_1. Therefore, the turn-off threshold is calculated as follows:

$$V_{\text{off}} = \frac{R_1R_2 + R_1R_4 + R_2R_4}{R_1R_2 + R_2R_4}\left[I_{n,\text{cr}}R_5 + V_{\text{T}} \ln\left(\frac{I_{n,\text{cr}}}{I_s}\right)\right]. \tag{6}$$

According to (5) and (6), V_{on} is higher than V_{off}, given the additional term R_1R_2 in the denominator in (6). One can adjust V_{on} and V_{off} offline by adjusting the resistance of R_1, R_2, and R_4.

2) Voltage Response Waveforms of the EBR: Fig. 3 records the voltage variation process of the EBR circuit and the subsequent voltage-regulation link, centrally reflecting the dynamic

Authorized licensed use limited to: ShanghaiTech University. Downloaded on November 09,2026 at 03:10:32 UTC from IEEE Xplore. Restrictions apply.

logic of "energy buffering-releasing." The key waveforms and stages are as follows.

1) *Energy Buffering Stage:* The input voltage v_{cst} of the EBR circuit (the voltage across the storage capacitor C_s) rises gradually from the initial value. In this stage, the EMU circuit is not activated, the output voltage v_o remains at 0, the control system is in a power-off state, and energy is continuously stored in C_s.
2) *Energy Release Triggering:* When v_{cst} rises to the preset turn-on threshold V_{on}, the switch M_1 in the EBR circuit is turned on, v_o jumps up instantaneously and synchronizes with v_{cst}. At the same time, energy is delivered to the low-dropout regulator (LDO), and the system starts.
3) *Maintenance and Turn-Off Stage:* After starting, V_{cst} decreases gradually due to energy release, and the EBR circuit remains in the on state. When V_{cst} drops to the preset turn-off threshold V_{off}, M_1 is turned off, v_o falls back to 0, the system stops operating, and waits for the next energy accumulation.

Hysteresis Formation Logic: The circuit needs to satisfy $V_{\text{cst}} \geq V_{\text{on}}$ to be turned on, and $V_{\text{cst}} \leq V_{\text{off}}$ to be turned off, and $V_{\text{on}} > V_{\text{off}}$ (in the document example, $V_{\text{on}} = 5.2\,\text{V}$, $V_{\text{off}} = 3.6\,\text{V}$). This voltage difference forms a hysteresis, avoiding frequent on-off of the circuit due to slight fluctuations of v_{cst}.

Connection With Circuit Design: The size of the hysteresis is determined by the voltage division relationship of resistors R_1, R_2, and R_4 (derived through Formulas 5 and 6). The adjustable hysteresis window can adapt to different capacities of the storage capacitor C_S, ensuring that the released energy is sufficient to complete the system start-up. Together, the two figures verify the core function of the EMU circuit: through a mechanism of "first buffering and storing energy, then triggering release."

To further optimize the energy efficiency of the above energy storage-release mechanism, appropriate operating mode selection is essential. In the research on the working mechanism of passive electronic devices, there are usually two typical working modes. Mode 1 is the intermittent working mode: after the energy storage is completed, the device starts to operate, and the energy storage operation is carried out again after the energy consumption is exhausted. This reciprocating process requires repeated initialization of the system, which not only reduces the energy utilization rate but also puts forward greater requirements for the capacity of the energy buffer capacitor. Mode 2 adopts the sleep mode to deal with the nonworking state, which can effectively reduce the energy consumption caused by repeated initialization, thereby improving the energy utilization rate. In view of this, Mode 2 is selected in this design.

In the design process of the EMU, the setting of the turn-on voltage V_{on} and turn-off voltage V_{off} thresholds is a core issue. The design shall be developed based on power consumption and capacitance capacity, with detailed derivation and explanation presented in Section III-C.

3) Design Example: We design an EM circuit targeting $V_{\text{on}} = 5.2$ V and $V_{\text{off}} = 3.6$ V. The initial step involves determining the transistors to be utilized. BSS84PW ($V_{\text{th},p} = -1.5\,\text{V}$) and MMBT3904 ($I_s = 4.36 \times 10^{-15}\,\text{A}$) are selected due to their cost-effectiveness. We initially set R_3 to 15 MΩ, such that $I_{n,\text{cr}} = |V_{\text{th},p}|/R_3$ approximates 100 nA. Configuring $I_{n,\text{cr}}$ to a relatively small magnitude is conducive to achieving a low quiescent current.

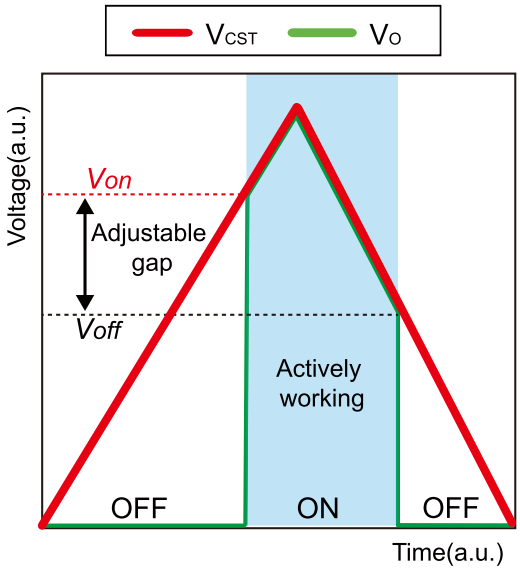


Fig. 3. Input and output voltage relationships for EBR.

Subsequently, R_5 is configured to ensure v_{b1} is approximately 0.6 V at the critical point. The main function of R_5 is to reduce the resistance values of R_1 and R_4. Substituting the known values into (2) yields $v_{b1} - v_{e1} = 0.43$ V. Since v_{e1} is approximately $I_{n,cr}R_5$, we can derive $R_5 = 1.5\,\text{MΩ}$. With this value of R_5, v_{b1} is approximately 0.57 V.

The subsequent step is to set the current across R_2 to be several times larger than $I_{n,\text{cr}}$, so that the base current of Q1 does not interfere with the voltage-dividing network while maintaining a low overall quiescent current. The current across R_2 is given by V_{b1}/R_2. In this case, R_2 is set to 2.4 MΩ. After that, R_1 and R_4 can be derived by substituting values into (5) and (6), and the results show $R_1 \approx 18\,\text{MΩ}$, $R_4 \approx 40\,\text{MΩ}$.

B. Software EM Using AEM

Hardware-defined thresholds exhibit an inherent limitation: once the circuit is fabricated, their values cannot be adjusted. For a more flexible EM to serve different software routines, an additional software-based scheme can make such a complement.

1) Core Principles and Operational Mechanisms: In this article, the AEM scheme deployed in the software layer achieves the balance between energy supply and demand. This balance is realized through a cyclic operation routine consisting of four sequential phases: energy testing, condition judgment, control execution, and adaptive adjustment. The cyclic operation of AEM is illustrated in Fig. 2(e). It can be elaborated by referring to the charging and discharging (loading) process shown in Fig. 4.

In Fig. 4, the black segments represent the charging periods, while the other colored segments represent the intermittent operating periods corresponding to different types of routines, as indicated by the legends in Fig. 4. The device begins to charge from a state of zero voltage and zero storage.

Authorized licensed use limited to: ShanghaiTech University. Downloaded on November 09,2026 at 03:10:32 UTC from IEEE Xplore. Restrictions apply.

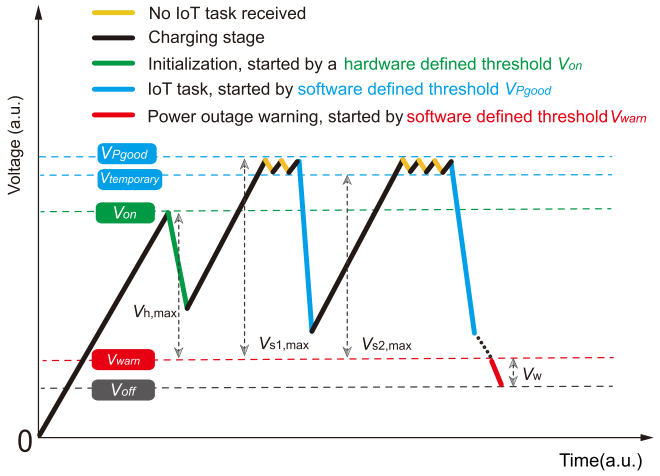


Fig. 4. Charging and discharging process of a self-powered electronic device with hardware–software collaborative management.

It cold-starts for initialization once the storage voltage attains the hardware start-up threshold V_{on}. Once initialization is complete, the device immediately enters sleep mode to conserve energy. The maximum usable energy for this initialization task is related to the hysteresis between V_{on} and V_{off}, which is denoted as $\Delta V_{\text{h, max}}$ in Fig. 4. After the hardware initialization, the MCU performs a scheduled sampling of the SoC by measuring the storage voltage using an ADC channel. An atomic IoT task is executed only when the estimated storage voltage exceeds the software-defined threshold V_{Pgood}, which indicates a power good condition. When the estimated storage voltage is lower than the software-defined warning threshold V_{warn}, the device sends out an alert packet to the host. The maximum usable energy for the most energy-consuming IoT task is related to the hysteresis between V_{Pgood} and V_{warn}, which is denoted as $\Delta V_{\text{s1, max}}$ in Fig. 4.

During the energy feedback phase, if the terminal device fails to receive the IoT task issued by the host device, or the host device is in an offline state, it shall maintain two core states: 1) continuously initiating energy feedback communication with the host device (this part of energy is denoted as $V_{\text{temporary}}$ in Fig. 4) and 2) reserving sufficient energy to complete the IoT task execution (this part of energy is denoted as $\Delta V_{\text{s2, max}}$ in Fig. 4). Finally, at any time the storage voltage drops below the hardware shutdown threshold V_{off}, the hardware EBR cutsoff the power supply. The system halts and undergoes another cold start. This process continues until the voltage rises back to V_{on}.

Through this hardware–software synergetic EM, the energy matching between the ambient energy source and electronic load demand is dynamically maintained. Such a sustainable operation is inevitably intermittent, given the volatile nature of an ambient energy source. Close monitoring of its SoC is a must for all self-powered devices.

2) Design Example: For the present experiment, the AEM software routine—schematically illustrated in Fig. 2(e)—is designed for in-program adjustment. This adjustment is achieved by adapting the routine to different load energy demands.

First, the total energy consumption of the entire communication cycle between the SP-Eink node and the host node was measured using a current analyzer. Subsequently, the system operation process within this cycle was decomposed in a modular manner, where three core subtasks were identified: initialization, SP-Eink communication and refresh display, and warning transmission. Next, independent energy consumption tests were conducted for each subtask during their operation, and the selection of capacitor capacity was completed based on the measured energy consumption data. Finally, relying on the energy consumption test data of each subtask and the selected capacitor parameters, exclusive start-up voltage thresholds (i.e., V_{Pgood} and V_{warn}) were configured for each subtask at the software level. The detailed design for threshold selection is referenced in the subsequent Section III-C. This configuration achieves precise matching between energy supply and task requirements, thereby completing the optimized design of voltage parameters for the AEM algorithm.

Algorithm 1 Working Logic of SP-Eink Nodes

```
set V_off < V_warn < V_on < V_pgood ;
when the circuit reaches the turn-on voltage V_on;
initialization of MCU ;
initialization of 2.4g module ;
2.4GHz module enters low-power sleep mode ;
initialization of Eink module ;
Eink module enters low-power sleep mode ;
while true do
    ADC sampling of V_sen ;
    if V_sen ≥ V_pgood then
        Wake up 2.4G module;
        2.4g module sends command A ;
        if No IoT task received from host then
            return to check V_sen ≥ V_pgood condition ;
        else
            Enter sleep mode after successful
             communication;
            Eink refreshes the received information ;
            Eink module enters low-power sleep mode ;
        end
    else if V_sen ≤ V_warn then
        Wake up 2.4G module;
        2.4g module sends alarm command B ;
        Enter sleep mode after successful
         communication;
end
```

The working logic between the SP-Eink node and the host, which is based on the AEM algorithm, is described as follows. Algorithm 1 defines the working logic of the SP-Eink node, and its core lies in a scheduling mechanism based on the AEM algorithm. Algorithm 2 specifies the working logic of the host. The design of these two algorithms enables bidirectional information interaction between the node and the host. This interaction covers multiple functions, including IoT task transmission, energy status monitoring, and operational fault detection.

Authorized licensed use limited to: ShanghaiTech University. Downloaded on November 09,2026 at 03:10:32 UTC from IEEE Xplore. Restrictions apply.

Algorithm 2 Working Logic of Host Node

```
initialization of MCU ;
initialization of 2.4g module ;
while true do
    Wait for interrupt trigger;
    Get interrupt flags;
    Read data from FIFO to RxBuf ;
    Check the command identifier in RxBuf ;
    if command A then
        Send SP-Eink display information data;
        Record command A;
    else if command B then
        Record the low-energy warning state of the
         SP-Eink node;
end
```

The design of the two algorithms supports bidirectional information interaction between nodes and the host. This interaction implements multiple functions, including IoT task transmission, energy status monitoring, and operational fault detection.

C. Theoretical Derivation and Analysis of Thresholds

This section elaborates on the theoretical derivation and analysis of multilevel energy thresholds for BF systems. It consists of four subparts: self-sustainability and feasibility boundary, threshold window constraints and derivation, example derivation and practical optimization, and reference design and scalability. First, the self-sustainability criterion and feasible threshold domain for the system's intermittent operation are clarified. Subsequently, energy windows at all levels and their constraint conditions are defined, and the minimum theoretical values of each threshold are derived accordingly. On this basis, combined with practical engineering operating conditions, the derivation and engineering optimization of threshold parameters are completed for the SP-Eink prototype. Finally, the general reference value and multiscenario scalability of the proposed architecture are illustrated.

1) Self-Sustainability and Feasibility Boundary: To quantify the ambient energy required for continuous intermittent operation, a complete operating cycle is defined as follows. The energy storage capacitor charges from the hardware turn-off threshold V_{off} to V_{on}, and the system enters initialization. Upon completion of initialization, task execution is triggered when the capacitor voltage reaches the software ready threshold V_{pgood}. When the capacitor voltage drops to the warning threshold, the capacitor discharges, and its voltage falls back to V_{off}.

The core self-sustainability criterion mandates that the total harvested energy during the charging phase must cover the total energy consumption of one full cycle

$$P_{\text{harvest_avg}} \cdot T_{\text{charge}} \geq E_{\text{init}} + E_{\text{warn}} + E_{\text{task}} \tag{7}$$

where $P_{\text{harvest_avg}}$ denotes the average ambient harvesting power during the charging phase, T_{charge} denotes the charging duration of one operation cycle, and E_{init}, E_{task}, and E_{warn} represent the energy consumption of cold-start initialization, core task execution, and low-energy warning transmission, respectively.

This work adopts a sleep-mode operation scheme. The full initialization procedure is performed only at the first cold start. Subsequent cycles remain in a low-power sleep state without repeated initialization, involving only task execution and warning transmission. Therefore, the practical self-sustainability condition is relaxed and is given by

$$P_{\text{harvest_avg}} \cdot T_{\text{charge}} \geq E_{\text{task}} + E_{\text{warn}}. \tag{8}$$

The software-ready threshold V_{pgood} is constrained by an explicit feasible domain

$$V^*_{\text{pgood}} \leq V_{\text{pgood}} \leq V_{\text{max}} \tag{9}$$

where V^*_{pgood} denotes the minimum feasible threshold for reliable task completion, which serves as the lower bound of the feasible domain and is derived in Section III-C2. V_{max} represents the maximum withstand voltage of the storage capacitor and front-end circuitry.

A core tradeoff exists between threshold setting and system performance. Raising V_{pgood} expands the voltage and energy margin, reduces the risk of midtask power failure, and enhances operational robustness. However, it also prolongs the charging duration of each cycle and increases capacitor leakage loss. Accordingly, the threshold should be adapted to ambient energy conditions.

2) Threshold Window Constraints and Derivation: The quantitative design of multilevel voltage thresholds forms the foundation for the lower bound of the feasible domain and reliable system operation. The closed-form constraints of multilevel energy windows and the corresponding minimum feasible thresholds are derived in this section, which serve as the design basis for AEM. These constraints are established based on the hardware threshold range, the capacity of the buffer capacitor, and the energy requirement of each system workflow.

Based on the fundamental energy storage formula for capacitors

$$E = \frac{1}{2}CU^2. \tag{10}$$

The total hardware energy window ΔV_h must cover the sum of the system initialization energy consumption and warning energy consumption ($E_{\text{init}} + E_{\text{warn}}$). As the system's survival baseline, ΔV_h ensures that once activated, the system can complete the full workflow of "cold start → energy warning transmission" even without any tasks. This eliminates unexpected midoperation failures

$$\Delta V_h = V_{\text{on}} - V_{\text{off}}. \tag{11}$$

The software task energy window ΔV_s must cover the sum of task execution energy consumption and warning energy consumption ($E_{\text{task}} + E_{\text{warn}}$). As a prerequisite for task execution, it ensures that the additional energy accumulated beyond hardware start-up can complete the full workflow of "core task execution → final warning transmission." This eliminates power failures during task execution

$$\Delta V_s = V_{\text{pgood}} - V_{\text{off}}. \tag{12}$$

Authorized licensed use limited to: ShanghaiTech University. Downloaded on November 09,2026 at 03:10:32 UTC from IEEE Xplore. Restrictions apply.

The warning energy window ΔV_w must cover the warning energy consumption (E_{warn}). As the last line of defense for system state feedback, it ensures that when the voltage drops to V_{warn}, the remaining energy is sufficient to transmit a warning signal. Subsequently, an immediate hardware shutdown is executed

$$\Delta V_w = V_{\text{warn}} - V_{\text{off}}. \tag{13}$$

Substituting the capacitor energy formula into the aforementioned constraints, a 10% engineering safety margin is introduced to ensure reliability under worst case conditions [53]. Taking V_{off} as the baseline, each threshold is derived accordingly.

Warning threshold V^*_{warn}: The energy available in the warning window must cover the warning transmission with margin

$$\frac{1}{2}C\left(V^2_{\text{warn}} - V^2_{\text{off}}\right) \geq 1.1 \cdot E_{\text{warn}}. \tag{14}$$

Rearranging yields the minimum theoretical value

$$V^*_{\text{warn}} = \sqrt{V^2_{\text{off}} + \frac{2.2 \cdot E_{\text{warn}}}{C}}. \tag{15}$$

Hardware turn-on threshold V^*_{on}: The hardware energy window must support full initialization and subsequent warning

$$\frac{1}{2}C\left(V^2_{\text{on}} - V^2_{\text{off}}\right) \geq 1.1 \cdot (E_{\text{init}} + E_{\text{warn}}). \tag{16}$$

Solving for the minimum turn-on threshold

$$V^*_{\text{on}} = \sqrt{V^2_{\text{off}} + \frac{2.2 \cdot (E_{\text{init}} + E_{\text{warn}})}{C}}. \tag{17}$$

Software ready threshold V^*_{pgood}: The software task window must guarantee complete task execution and final feedback

$$\frac{1}{2}C\left(V^2_{\text{pgood}} - V^2_{\text{off}}\right) \geq 1.1 \cdot (E_{\text{task}} + E_{\text{warn}}). \tag{18}$$

The corresponding minimum threshold is

$$V^*_{\text{pgood}} = \sqrt{V^2_{\text{off}} + \frac{2.2 \cdot (E_{\text{task}} + E_{\text{warn}})}{C}}. \tag{19}$$

3) Example Derivation and Practical Optimization: The above Section III-C2 defines threshold window constraints and derivation for system EM. Nevertheless, the threshold values derived from theoretical analysis need to be comprehensively revised in combination with actual engineering operating conditions. Extreme working conditions, including component parameter tolerances, dynamic task energy consumption fluctuations, cold startups, and instantaneous power failures upon task completion, should be fully considered. Finally, threshold parameters that can be directly configured and adapted to practical systems are output.

In the design of threshold parameter selection for SP-Eink in this project, a 10% industrial standard safety margin is adopted. Theoretical thresholds are derived based on the defined energy window constraints. Using two parallel 1000 μF capacitors ($\pm$20% tolerance, $C_{\text{min}} = 1600\,\mu$F, low-leakage capacitors are connected in parallel. In accordance with industry standards, when charged at the rated voltage for 1 min, the maximum leakage current of a single capacitor is 160 μA; all calculations are conducted under the worst case condition. This approach ensures the reliability of the system while strictly retaining the core design parameters.

With a fixed system shutdown threshold $V_{\text{off}} = 3.6\,\text{V}$ and the measured power consumption data ($E_{\text{init}} = 7.76\,\text{mJ}$, $E_{\text{task}} = 9.87\,\text{mJ}$, and $E_{\text{warn}} = 0.2\,\text{mJ}$), the thresholds under the worst case condition are derived as follows.

Warning Threshold: The energy constraint for the warning window is

$$\frac{1}{2}C_{\text{min}}\left(V^2_{\text{warn}} - V^2_{\text{off}}\right) \geq 1.1 \cdot E_{\text{warn}}. \tag{20}$$

Solving for the minimum feasible value gives

$$V^*_{\text{warn}} = \sqrt{V^2_{\text{off}} + \frac{2.2 \cdot E_{\text{warn}}}{C_{\text{min}}}} \approx 3.64\,\text{V}. \tag{21}$$

Hardware Start-Up Threshold: The energy constraint for the hardware survival window is

$$\frac{1}{2}C_{\text{min}}\left(V^2_{\text{on}} - V^2_{\text{off}}\right) \geq 1.1 \cdot (E_{\text{init}} + E_{\text{warn}}). \tag{22}$$

Solving for the minimum feasible value gives

$$V^*_{\text{on}} = \sqrt{V^2_{\text{off}} + \frac{2.2 \cdot (E_{\text{init}} + E_{\text{warn}})}{C_{\text{min}}}} \approx 4.82\,\text{V}. \tag{23}$$

Software Ready Threshold: The energy constraint for the task execution window is

$$\frac{1}{2}C_{\text{min}}\left(V^2_{\text{pgood}} - V^2_{\text{off}}\right) \geq 1.1 \cdot (E_{\text{task}} + E_{\text{warn}}). \tag{24}$$

Solving for the minimum feasible value gives

$$V^*_{\text{pgood}} = \sqrt{V^2_{\text{off}} + \frac{2.2 \cdot (E_{\text{task}} + E_{\text{warn}})}{C_{\text{min}}}} \approx 5.10\,\text{V}. \tag{25}$$

Combining the foregoing theoretical derivation and practical engineering limitations, the experimental threshold values are specified as $V_{\text{on}} = 5.2\,\text{V}$, $V_{\text{off}} = 3.6\,\text{V}$, $V_{\text{pgood}} = 5.6\,\text{V}$, and $V_{\text{warn}} = 3.8\,\text{V}$. All these practical parameters are marginally larger than the corresponding theoretically calculated values. Such design margins are reserved to address unexpected operational scenarios including abrupt full shading occurring right after cold start-up. These reserved margins supply redundant buffer energy and prevent frequent early warnings as well as repeated system initialization. In addition, V_{pgood} is increased from its optimal theoretical value of 5.10 V to 5.6 V. This adjustment is made to support the diverse refreshing operations of SP-Eink modules. This customized design maintains steady system operation and alleviates performance deterioration originating from component discrepancies and manufacturing tolerances.

4) Reference Design and Scalability: The proposed hardware–software collaborative EM architecture exhibits favorable scalability. It adapts to various EH modalities [photovoltaic (PV), piezoelectric, and thermoelectric] through front-end rectifier replacement. It accommodates tasks with different power profiles by tuning the EBR circuit and software thresholds based on measured power characteristics.

Beyond BF application scenarios, this design also offers a certain reference value for IoT terminals equipped with small batteries, yet it cannot be directly copied. The reusable core

Authorized licensed use limited to: ShanghaiTech University. Downloaded on November 09,2026 at 03:10:32 UTC from IEEE Xplore. Restrictions apply.

TABLE II
POWER CONSUMPTION IN DIFFERENT PHASES

Working state	Energy consumption	Duration
Initialization	7.76 mJ	385 ms
Communication & E-ink refresh	9.87 mJ	1060 ms
Warning transmission	0.2 mJ	14 ms
ADC sampling	0.9 μJ	0.1 ms
No IoT task received	3.68 mJ	80 ms

ideas specifically include estimating the battery SoC through voltage sampling. It also involves adopting threshold control logic to reduce the number of system cold starts. This approach thereby slows down battery degradation and extends its service life.

IV. EXPERIMENTAL EVALUATION

The proposed hardware–software collaborative EM scheme is embodied and facilitates the development and operation of an SP-Eink display. The display carries out relatively complex tasks by using the scarce energy from the indoor light. Its operation is more sophisticated than the self-powered Bluetooth beacon nodes realized in the early studies [54], [55].

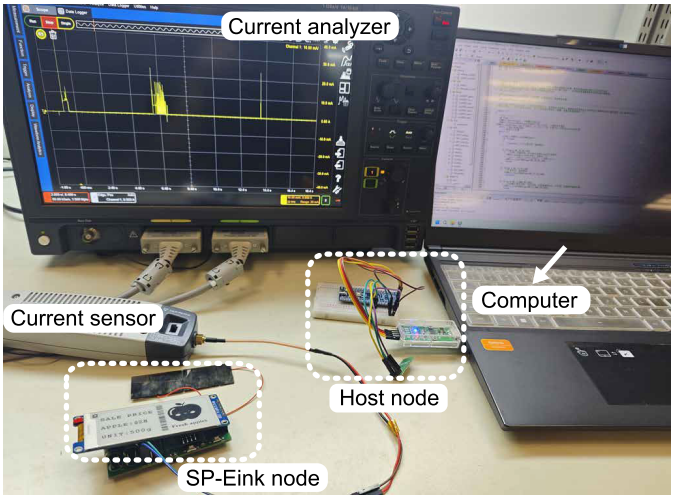
A. Energy Consumption

Fig. 5(a) presents the experimental setup and measured current waveform for the power consumption test of the prototyped SP-Eink display node. The experimental platform consists of a laptop, a host node, an SP-Eink node, two PV panels, and a CX3322A current analyzer manufactured by EsterTech. The host node communicates with the computer through a serial port and transmits display data to the SP-Eink node via a 2.4G wireless communication module. The current analyzer is employed to measure the operating current of the SP-Eink node during operation.

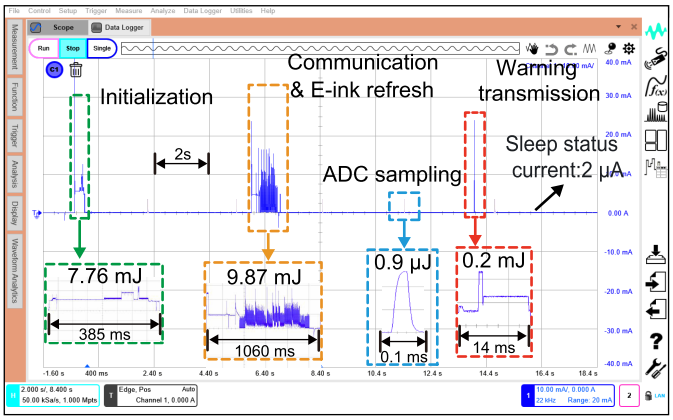
Fig. 5(b) and (c) respectively presents the power consumption measurement current graphs of the SP-Eink node for initial power-on initialization, communication and E-ink refresh, warning transmission, ADC sampling, and no host response received. Table II lists the measured energy consumption and duration of each core task. Although the energy required for E-ink operation is significantly higher than that of a single self-powered Bluetooth low energy (BLE) beacon device (approximately 10 versus 0.2 mJ [54]), periodic batch communication and E-ink refresh functions have been successfully implemented through a sophisticated hardware–software collaborative EM scheme.

B. Operational Robustness

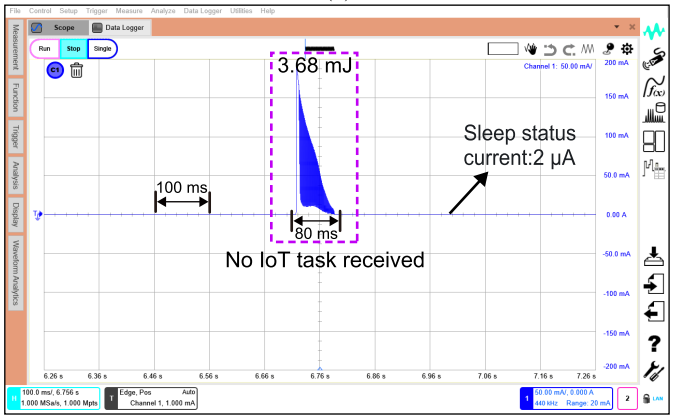
To further validate the proposed EM scheme under a volatile light source, another experiment is carried out under a continuous change of light intensity. The setup is shown in Fig. 6(a). An oscilloscope (DS1104Z by Rigol Ltd.) is used to monitor the storage voltage, which indicates the charging and discharging (loading) procedures. Each steep falling edge represents a discharge associated with a specific IoT task.



(a)



(b)



(c)

Fig. 5. Energy consumption testing of SP-Eink node. (a) Setup. (b) Energy consumption waveform at each process stage. (c) No IoT task received.

Fig. 6(b) illustrates that the SP-Eink node maintains excellent operational stability under diverse indoor illumination conditions. Its operation is regulated by a multilevel energy threshold control mechanism. When the voltage of the energy buffer capacitor rises to the turn-on threshold V_{on} of the EBR circuit, the system completes a single initialization and enters a sleep energy storage state. When the voltage reaches V_{pgood}, the SP-Eink node executes communication and refresh tasks. When the voltage drops to V_{warn}, the SP-Eink node sends an energy warning command to the host. The system only

Authorized licensed use limited to: ShanghaiTech University. Downloaded on November 09,2026 at 03:10:32 UTC from IEEE Xplore. Restrictions apply.

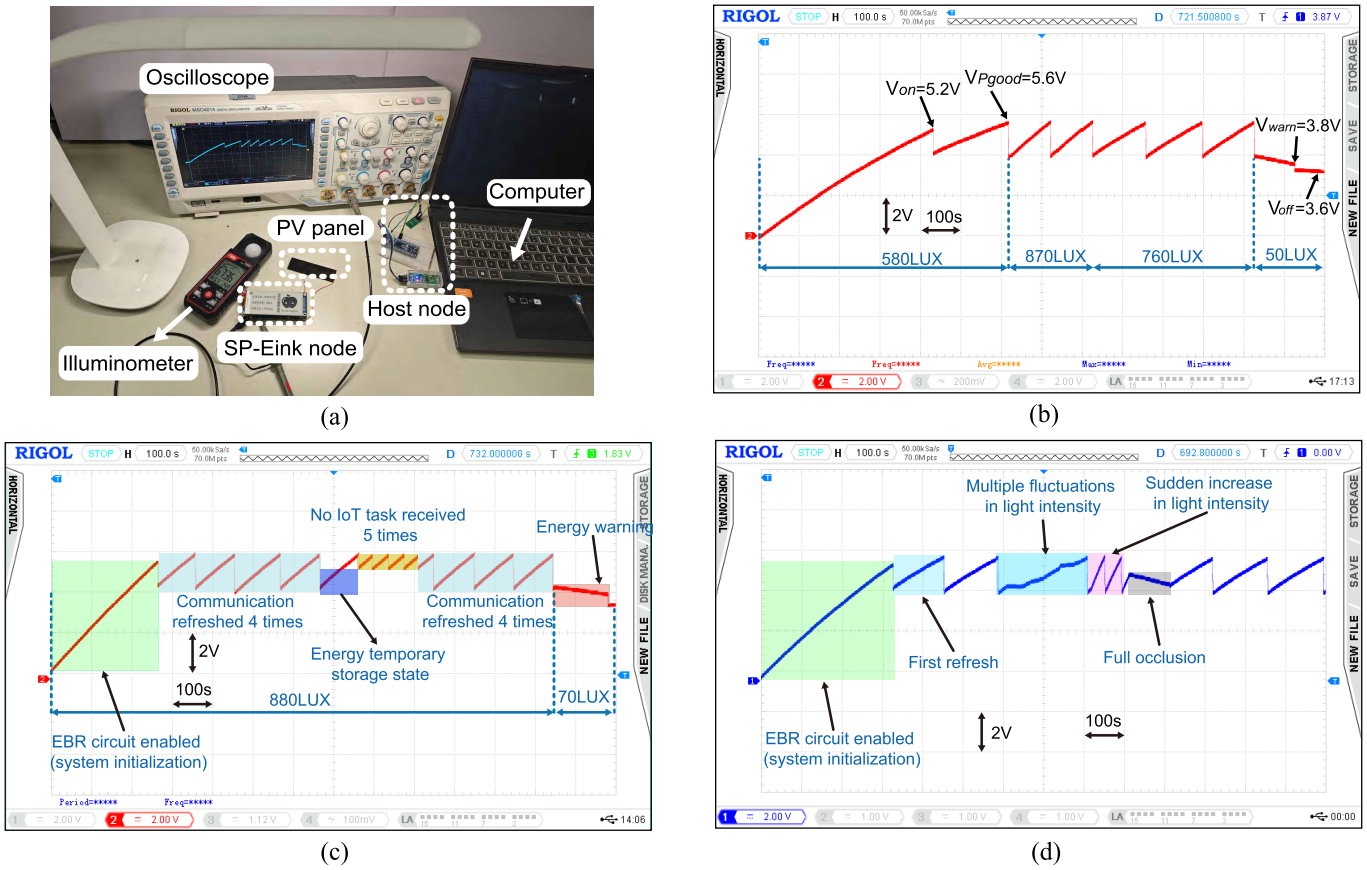


Fig. 6. System performance verification under varying illumination conditions. (a) Setup. (b) Intermittent operation voltage waveforms. (c) Task reception effect comparison. (d) Harsh scenario robustness test.

requires reinitialization under extreme operating conditions, such as full occlusion of the PV panel. This design enables remote monitoring of operating status and faults via the energy feedback mechanism of the terminal node. It further validates the superiority of the proposed hardware–software collaborative EM mechanism.

Fig. 6(c) presents the energy storage voltage waveforms of the SP-Eink node under different operating states. In particular, the green region corresponds to the node's energy storage and system initialization phase. The blue region represents the normal host communication and screen refresh phase. To verify the energy feedback mechanism under communication and task reception failure scenarios, an experiment was conducted with the host in an offline condition. The waveform in the yellow region indicates that, when no task is issued by the host, the node enters an energy temporary storage state (dark blue region). It reserves the energy required for E-ink screen refresh and continuously sends task request commands to the host until the host returns online. The red region represents the node's energy warning phase. This design enables real-time feedback of the node's energy consumption status. It also effectively avoids invalid energy consumption when no tasks are available.

Fig. 6(d) presents the robustness test results of the SP-Eink node under harsh energy supply conditions. The waveform shows that the system maintains stable operation during multiple light intensity fluctuations and sudden increases in illumination. When full light occlusion occurs (gray region), no light energy is supplied at this moment, and the energy buffer capacitor enters a full discharge state. It seamlessly resumes normal operation immediately after the light source is restored, avoiding unnecessary reinitialization and energy waste. These results verify that the proposed hardware–software collaborative EM mechanism can effectively adapt to unstable energy input scenarios. This significantly enhances the practical applicability of self-powered IoT devices.

C. Multinode SP-Eink Offline Test

To comprehensively validate the functionality and performance of the wireless SP-Eink device, an integrated prototype was designed, as illustrated in Fig. 7. The hardware components of the SP-Eink node are enumerated in Fig. 7(a). These components specifically include two PV boards, one printed circuit board (PCB) module, and one E-ink module. Fig. 7(b) presents an integrated prototype of the SP-Eink node. Two PV boards, which serve as energy storage and power supply, are mounted on the top of this prototype. The shell structure of the prototype is fabricated using polylactic acid as the raw material, with a 3-D printer employed as the manufacturing tool. In particular, the dimensions of the prototype shell are determined to be 97 × 45 × 22 mm. The parameters of the

Authorized licensed use limited to: ShanghaiTech University. Downloaded on November 09,2026 at 03:10:32 UTC from IEEE Xplore. Restrictions apply.

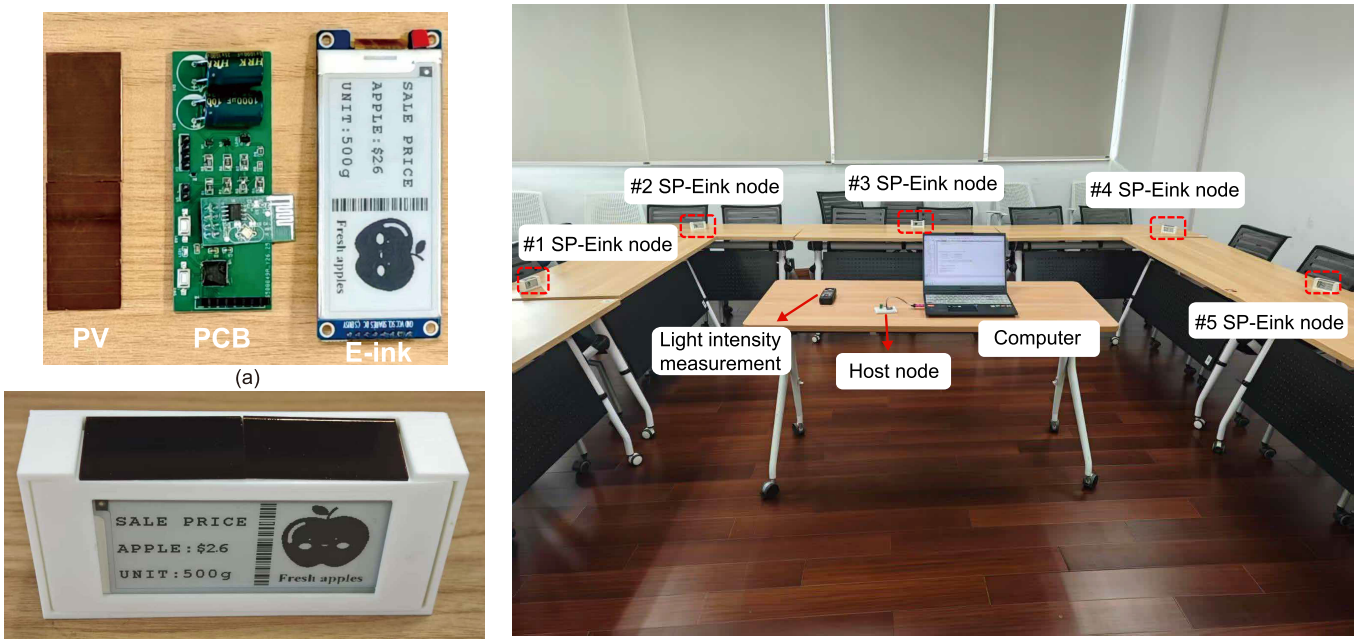


Fig. 7. SP-Eink node prototype and field test.

TABLE III
MAIN COMPONENTS AND PARAMETERS OF SP-EINK NODES

Component	Value / Type
Photovoltaic panel	$37 \times 21 \times 1.1$ mm $\times$ 2
R1, R2, R3, R4, R5	18, 2.4, 15, 40, 1.5 MΩ
Energy buffer capacitor	1000μF $\times$ 2
LDO	TPS70933DBVR
NPN	MMBT3904
PMOS	BSS84PWH6327
Diode	1N4148WS
MCU	CW32L031
2.4G module	PAN2110
E-ink	2.9 inches
R6, R7, R8	5 MΩ,10 MΩ,10 KΩ
LED	NCD0603R1
C1, C2, C3	4.7μF, 100nF, 100nF
Key1, Key2	TS-1101-C-W, TS-1101-C-W

TABLE IV
SP-EINK NODES EXPERIMENTAL TEST RESULTS

No.	light intensity	Refresh time	Energy feedback
1	150 LUX	22.6 min	100%
2	250 LUX	12.5 min	100%
3	350 LUX	7.8 min	100%
4	450 LUX	4.5 min	100%
5	550 LUX	3.1 min	100%
6	650 LUX	2.5 min	100%
7	750 LUX	2.1 min	100%
8	850 LUX	1.6 min	100%

main components corresponding to each part of the SP-Eink node are listed in Table III.

Fig. 7(c) presents the field test of the SP-Eink node. For the experimental tests, a conference room with dimensions of 5×5 m was selected as the test scenario. Both the host node and terminal nodes employed 2.4-GHz communication. The host node was deployed at the center of the communication area, with responsibilities including monitoring the entire network and interacting with the computer through the serial port. Detailed test results are presented in Table IV.

Experimental results demonstrate that the host node and all terminal SP-Eink nodes can maintain reliable communication even under a low-light environment of 150 lux. This work verifies the stability of the communication link for BF terminal nodes to transmit energy status and operating parameters back to the host node in a multinode networking scenario. Meanwhile, the energy status feedback function of each SP-Eink node is also validated.

D. Comparative Analysis of Performance and Cost Benefits

The quantitative tradeoff between performance gain and implementation cost serves as the core evaluation metric for EM schemes. The comparison is performed from two dimensions: performance and cost. From both performance and cost perspectives, the hardware–software codesigned EM scheme proposed in this article is quantitatively compared with the pure hardware UVLO chip BQ25570. This chip is widely adopted in the EH field. The comparative results are presented in Table V.

1) Performance Analysis: The proposed scheme delivers remarkable improvements in operational efficiency, functionality, and reliability. At 350 lux, it reduces the average refresh interval by 40.9% (nearly doubling the update frequency). Hardware leakage current is reduced by 71.3%. Moreover, the scheme integrates real-time energy feedback and adjustable thresholds to improve monitoring performance and system adaptability. In addition, it limits the number of initializations

Authorized licensed use limited to: ShanghaiTech University. Downloaded on November 09,2026 at 03:10:32 UTC from IEEE Xplore. Restrictions apply.

TABLE V
PERFORMANCE COMPARISON AND COST-BENEFIT ANALYSIS

Category	Indicator	Pure hardware (BQ25570)	Proposed	Relative change
Performance	Refresh interval @ 350 lux	13.2 min	7.8 min	-40.9%
	Energy feedback	None	Available	New
	Threshold adjustability	Partially programmable	Adjustable	New
	Leakage current(BQ25570 vs EBR)	0.48 μA	0.14 μA	-71.3%
	Initializations per cycle	Every power-up	Once at cold start	Reduced
Cost	Hardware BOM cost	\$14.2	\$6.95	-51.1%
	Storage capacitance	4700 μF	2000 μF	-57.4%
	Core device volume	Larger	Smaller	Reduced
	Implementation complexity	Medium	Medium	Comparable

per cycle to a single cold start. This design eliminates energy waste and reliability risks caused by frequent cold starts.

2) Cost Analysis: It reduces the hardware BOM cost by 51.1% via a discrete-component design. The required storage capacitance is decreased by 57.4%. Meanwhile, its implementation complexity is comparable to that of commercial pure hardware solutions. This feature guarantees satisfactory engineering practicability.

3) Comprehensive Analysis: Experimental comparison results show that the proposed scheme achieves better performance and higher cost-effectiveness than traditional pure hardware UVLO schemes. This validates the advantages of the hardware–software collaborative design.

Furthermore, conventional dynamic switching EM strategies based on preset task cycles are constrained by fixed cycle configurations. They struggle to adapt to abrupt fluctuations in environmental energy and lack differentiated optimization for various scenarios. As a result, the overall task efficiency is generally limited under conditions of unstable energy supply. On the contrary, the AEM scheme can sense the energy storage status in real time and execute corresponding tasks. Thus, it exhibits more prominent advantages in scenario adaptability and energy utilization efficiency. In general, the proposed scheme complies with the BF IoT principle of "maximizing benefits with minimal overhead" and possesses good practical engineering value.

V. CONCLUSION

This article introduced a hardware–software collaborative EM scheme for reliable start-up and operation of BF electronic devices. At the hardware level, an EBR circuit is employed. This circuit provides hardware-defined voltage thresholds. These thresholds ensure the minimum required operation of the system. The operation covers the range from passive cold start to system shutdown. At the software level, an AEM scheme is developed. It complements the EBR by bringing flexibility to the threshold adjustment. Two additional software-defined thresholds are adjustable according to the working condition in cyclic operation routines. It realizes an adaptive energy budget for ensuring the successful run of IoT tasks with different energy demands. Furthermore, when no task is received from the host, each SP-Eink node establishes cyclic communication with the host, which not only preserves the energy required for node display refresh but also feeds back its own energy status, providing reliable data support for the system's energy storage, monitoring, and fault diagnosis. Currently, this collaborative EM scheme has been specifically embodied and implemented in a prototyped SP-Eink node. Its stability in the operation of the SP-Eink device has been verified under varying light source conditions, providing a potentially valuable technical solution for the development and promotion of sustainable wireless SP-Eink and ubiquitous self-powered electronic devices.

REFERENCES

[1] B. H. Zeng, S. Y. Zheng, and W. S. Chan, "Single- and wide-band cooperative rectifiers harvesting ambient electromagnetic-photovoltaic energy for powering battery-less sensors," *IEEE Internet Things J.*, vol. 12, no. 14, pp. 26569–26581, Jul. 2025.

[2] J. Li et al., "A real-time hierarchical energy management strategy for FTPSS to improve the PV/RBE utilization and power supply quality," *IEEE Trans. Intell. Transp. Syst.*, vol. 26, no. 1, pp. 1203–1214, Jan. 2025.

[3] N. Rezaei-Hosseinabadi, A. Amoorezaei, A. Tabesh, S. A. Khajehoddin, R. Dehghani, and K. Moez, "A voltage-feedback-based maximum power point tracking technique for piezoelectric energy harvesting interface circuits," *IEEE Internet Things J.*, vol. 11, no. 11, pp. 20433–20442, Jun. 2024.

[4] W. Gong et al., "Embracing self-powered wearables for intelligent healthcare data management," *IEEE Internet Things J.*, vol. 11, no. 15, pp. 25674–25681, Aug. 2024.

[5] L. Miuccio, D. Panno, S. Riolo, and A. Schilirò, "Reliable and energy-efficient MAC protocols in industrial IoT networks via multi-agent reinforcement learning," *IEEE Trans. Mach. Learn. Commun. Netw.*, vol. 4, pp. 677–705, 2026.

[6] J. Meng, J. Qiu, and J. Liang, "Hardware and software collaborative energy management for a light-powered E-ink display," in *Proc. IEEE Int. Symp. Circuits Syst. (ISCAS)*, May 2026, pp. 3793–3797.

[7] N. Rathi and K. Roy, "LITE-SNN: Leveraging inherent dynamics to train energy-efficient spiking neural networks for sequential learning," *IEEE Trans. Cognit. Develop. Syst.*, vol. 16, no. 6, pp. 1905–1914, May 2024.

[8] L. Miuccio, D. Panno, and S. Riolo, "An energy-efficient DL-aided massive multiple access scheme for IoT scenarios in beyond 5G networks," *IEEE Internet Things J.*, vol. 10, no. 9, pp. 7936–7959, May 2023.

[9] T. Ji, Y. Guo, Q. Wang, X. Wang, and P. Li, "ECONOMY: Point clouds-based energy-efficient autonomous navigation for UAVs," *IEEE Trans. Netw. Sci. Eng.*, vol. 8, no. 4, pp. 2885–2896, Oct. 2021.

[10] A. Chakraborty and A. Maity, "A battery-less energy harvesting front-end for powering multiple IoT nodes using single solar cell: A system-level perspective," *IEEE Trans. Power Electron.*, vol. 40, no. 9, pp. 14072–14083, Sep. 2025.

[11] K. Hammoud et al., "Efficient light energy harvesting and RF distribution for dense IoT networks," *IEEE Internet Things J.*, vol. 13, no. 7, pp. 15005–15019, Apr. 2026.

[12] A. Leoni, D. Colaiuda, V. Stornelli, and G. Ferri, "A novel ultralow-power, battery-less BLE plant monitoring, and energy harvesting system," *IEEE Internet Things J.*, vol. 13, no. 7, pp. 12851–12862, Apr. 2026.

Authorized licensed use limited to: ShanghaiTech University. Downloaded on November 09,2026 at 03:10:32 UTC from IEEE Xplore. Restrictions apply.

[13] J. J. Estrada-López, A. A. Castillo-Atoche, J. Vázquez-Castillo, and E. Sánchez-Sinencio, "Smart soil parameters estimation system using an autonomous wireless sensor network with dynamic power management strategy," *IEEE Sensors J.*, vol. 18, no. 21, pp. 8913–8923, Nov. 2018.

[14] G. Shi et al., "An Internet of Things management system for roadside parking space based on solar power supply and RF energy transmission," *IEEE Internet Things J.*, vol. 11, no. 6, pp. 10224–10238, Mar. 2024.

[15] S. Shen, Y. Zhang, C.-Y. Chiu, and R. Murch, "Directional multiport ambient RF energy-harvesting system for the Internet of Things," *IEEE Internet Things J.*, vol. 8, no. 7, pp. 5850–5865, Apr. 2021.

[16] A. Luo et al., "Vibration energy harvester with double frequency-up conversion mechanism for self-powered sensing system in smart city," *Nano Energy*, vol. 105, Jan. 2023, Art. no. 108030.

[17] K. Qian, H. Xia, and Y. Xia, "A self-powered interface circuit for piezoelectric and photovoltaic energy extracting," *Microelectron. J.*, vol. 154, Dec. 2024, Art. no. 106466.

[18] M. Götz and O. Kanoun, "Ultralow power voltage supervisor for ambient power-driven microcontroller systems," *IEEE Trans. Ind. Electron.*, vol. 66, no. 5, pp. 3843–3851, May 2019.

[19] X. Tang, X. Liu, G. Xie, Y. Cui, and D. Li, "Prototype implementation and experimental evaluation for LoRa-backscatter communication systems with RF energy harvesting and low power management," *IEEE Trans. Commun.*, vol. 73, no. 7, pp. 4811–4825, Jul. 2025.

[20] L. Miuccio, D. Panno, and S. Riolo, "A flexible encoding/decoding procedure for 6G SCMA wireless networks via adversarial machine learning techniques," *IEEE Trans. Veh. Technol.*, vol. 72, no. 3, pp. 3288–3303, Mar. 2023.

[21] Y.-Y. Huang, M. Takamiya, and P.-H. Chen, "Serial-stacked single-inductor dual-source triple-output energy harvesting interface with 2D-MPPT for battery-free IoT devices," *IEEE Trans. Circuits Syst. I, Reg. Papers*, vol. 72, no. 11, pp. 6592–6603, Nov. 2025.

[22] P.-H. Chen, T.-Y. Su, and P. M.-Y. Fan, "Thermoelectric energy harvesting interface circuit with capacitive bootstrapping technique for energy-efficient IoT devices," *IEEE Internet Things J.*, vol. 5, no. 5, pp. 4058–4065, Oct. 2018.

[23] M. Cai and W.-H. Liao, "A coaxial Wrist–Worn energy harvester for self-powered Internet of Things sensors," *IEEE Internet Things J.*, vol. 10, no. 1, pp. 133–143, Jan. 2023.

[24] I. Lee, Y. Lee, D. Sylvester, and D. Blaauw, "Battery voltage supervisors for miniature IoT systems," *IEEE J. Solid-State Circuits*, vol. 51, no. 11, pp. 2743–2756, Nov. 2016.

[25] Z. Chen, L. Teng, L. Xu, J. Yu, and J. Liang, "MP-HAR: A novel motion-powered real-time human activity recognition system," *IEEE Internet Things J.*, vol. 11, no. 5, pp. 7652–7663, Mar. 2024.

[26] L. Miuccio, S. Riolo, S. Samarakoon, M. Bennis, and D. Panno, "On learning generalized wireless MAC communication protocols via a feasible multi-agent reinforcement learning framework," *IEEE Trans. Mach. Learn. Commun. Netw.*, vol. 2, pp. 298–317, 2024.

[27] S. Vastrad and K. R. Shobha, "Power-efficient trickle algorithm with dynamic adjustment of idle interval for Internet-of-Things application," *IEEE Sensors J.*, vol. 24, no. 3, pp. 3853–3862, Feb. 2024.

[28] A. Sabovic, A. K. Sultania, C. Delgado, L. D. Roeck, and J. Famaey, "An energy-aware task scheduler for energy-harvesting batteryless IoT devices," *IEEE Internet Things J.*, vol. 9, no. 22, pp. 23097–23114, Nov. 2022.

[29] M. R. Elhebeary, M. A. A. Ibrahim, M. M. Aboudina, and A. N. Mohieldin, "Dual-source self-start high-efficiency microscale smart energy harvesting system for IoT," *IEEE Trans. Ind. Electron.*, vol. 65, no. 1, pp. 342–351, Jan. 2018.

[30] A. K. Sultania and J. Famaey, "Batteryless Bluetooth low energy prototype with energy-aware bidirectional communication powered by ambient light," *IEEE Sensors J.*, vol. 22, no. 7, pp. 6685–6697, Apr. 2022.

[31] L. Teng, H. Wang, Y. Liu, M. Fu, and J. Liang, "A three-transistor energy management circuit for energy-harvesting-powered IoT devices," *IEEE Internet Things J.*, vol. 11, no. 1, pp. 1301–1310, Jan. 2024.

[32] T. Ruan, Z. J. Chew, and M. Zhu, "Energy-aware approaches for energy harvesting powered wireless sensor nodes," *IEEE Sensors J.*, vol. 17, no. 7, pp. 2165–2173, Apr. 2017.

[33] E. Dallago, A. L. Barnabei, A. Liberale, P. Malcovati, and G. Venchi, "An interface circuit for low-voltage low-current energy harvesting systems," *IEEE Trans. Power Electron.*, vol. 30, no. 3, pp. 1411–1420, Mar. 2015.

[34] A. Talgat, M. A. Kishk, and M.-S. Alouini, "Maximizing uplink data transmission of LEO-satellite-based wireless-powered IoT," *IEEE Internet Things J.*, vol. 11, no. 17, pp. 28975–28987, Sep. 2024.

[35] D. Kumar, C. K. Singh, O. L. A. López, V. Bhatia, and M. Latva-Aho, "Performance analysis of passive/active RIS aided wireless-powered IoT network with nonlinear energy harvesting," *IEEE Trans. Wireless Commun.*, vol. 24, no. 2, pp. 1132–1145, Feb. 2025.

[36] D. Lin, J. Wan, J. Wang, L. Kong, Y. Zhao, and Y. L. Guan, "A novel topology-scale-adaptive and energy-efficient clustering scheme for energy sustainable large-scale SWIPT-enabled WSNs," *IEEE Trans. Mobile Comput.*, vol. 23, no. 12, pp. 13172–13188, Dec. 2024.

[37] Y. Zhang, S. He, and J. Chen, "Data gathering optimization by dynamic sensing and routing in rechargeable sensor networks," *IEEE/ACM Trans. Netw.*, vol. 24, no. 3, pp. 1632–1646, Jun. 2016.

[38] A. Hentati, Z. Mlika, J.-F. Frigon, and W. Ajib, "Energy harvesting wireless sensor networks: Inter-delivery-aware scheduling algorithms," in *Proc. IEEE Wireless Commun. Netw. Conf. (WCNC)*, Apr. 2022, pp. 1135–1139.

[39] Y. Wang, J. Qiu, M. Fu, H. Wang, and J. Liang, "ViPSN-button: A motion-powered wireless pushbutton with instant feedback," *IEEE Internet Things J.*, vol. 12, no. 24, pp. 54791–54803, Dec. 2025.

[40] D. Jiao, P. Yang, L. Fu, L. Ke, and K. Tang, "Optimal energy-delay scheduling for energy-harvesting WSNs with interference channel via negatively correlated search," *IEEE Internet Things J.*, vol. 7, no. 3, pp. 1690–1703, Mar. 2020.

[41] K. Agrawal, S. Prakriya, and K. Singh, "Performance of a new dynamic time-switching protocol with a battery-assisted FD relay," in *Proc. IEEE 97th Veh. Technol. Conf. (VTC-Spring)*, Jun. 2023, pp. 1–7.

[42] F. Salvadori et al., "Monitoring in industrial systems using wireless sensor network with dynamic power management," *IEEE Trans. Instrum. Meas.*, vol. 58, no. 9, pp. 3104–3111, Sep. 2009.

[43] G. Loubet, J.-P. Balayssac, A. Sidibe, D. Dragomirescu, and A. Takacs, "Battery-free, wirelessly powered and controlled concrete resistivity sensing node," in *Proc. Wireless Power Week (WPW)*, Jul. 2022, pp. 547–552.

[44] S. Qiu, Y.-H. Zhu, X. Tian, and K. Chi, "Goodput-maximised data delivery scheme for battery-free wireless sensor network," *IET Commun.*, vol. 14, no. 4, pp. 665–673, Mar. 2020.

[45] Y.-H. Zhu, E. Li, and K. Chi, "Encoding scheme to reduce energy consumption of delivering data in radio frequency powered battery-free wireless sensor networks," *IEEE Trans. Veh. Technol.*, vol. 67, no. 4, pp. 3085–3097, Apr. 2018.

[46] K. Chen, H. Gao, Z. Cai, Q. Chen, and J. Li, "Distributed energy-adaptive aggregation scheduling with coverage guarantee for battery-free wireless sensor networks," in *Proc. IEEE INFOCOM Conf. Comput. Commun.*, Apr. 2019, pp. 1018–1026.

[47] Y. Kim, Y. S. Park, H. G. Lee, and D. Baek, "Designing cost-effective battery-less energy harvesting for intermittent wireless communication," *IEEE Access*, vol. 13, pp. 157044–157058, 2025.

[48] C.-C. Huang and C.-L. Lin, "Wireless power and bidirectional data transfer scheme for battery charger," *IEEE Trans. Power Electron.*, vol. 33, no. 6, pp. 4679–4689, Jun. 2018.

[49] M. Keller et al., "Robust temperature change rate actuated valving and switching for highly integrated centrifugal microfluidics," *Lab Chip*, vol. 17, no. 5, pp. 864–875, 2017.

[50] P. C. Sekar and H. Mangalam, "A power aware mechanism for energy efficient routing in MANET," *Int. J. Netw. Virtual Organisations*, vol. 21, no. 1, pp. 3–18, 2019.

[51] D. Senapati, A. Sarkar, and C. Karfa, "Energy-aware real-time scheduling of multiple periodic DAGs on heterogeneous systems," *IEEE Trans. Comput.-Aided Design Integr. Circuits Syst.*, vol. 42, no. 8, pp. 2447–2460, Aug. 2023.

[52] V. Fernandes, N. Cravo, H. L. M. Monteiro, D. N. K. Jayakody, H. V. Poor, and M. V. Ribeiro, "Energy harvesting in the UNB-PLC spectrum: Hidden opportunities for IoT devices," *IEEE Internet Things J.*, vol. 10, no. 2, pp. 1236–1247, Jan. 2023.

[53] P. D. T. O. Connor, "U. S. military handbook 338: Electronic reliability design Handbook. Available from the U.S. national technical information center, springfield, Virginia. (In the U.K. from London information, index house, ascot, Berkshire)," *Qual. Rel. Eng. Int.*, vol. 2, no. 2, p. 139, Apr. 1986.

[54] X. Li et al., "ViPSN: A vibration-powered IoT platform," *IEEE Internet Things J.*, vol. 8, no. 3, pp. 1728–1739, Feb. 2021.

[55] X. Li, H. Tang, G. Hu, B. Zhao, and J. Liang, "ViPSN-pluck: A transient-motion-powered motion detector," *IEEE Internet Things J.*, vol. 9, no. 5, pp. 3372–3382, Mar. 2022.

Authorized licensed use limited to: ShanghaiTech University. Downloaded on November 09,2026 at 03:10:32 UTC from IEEE Xplore. Restrictions apply.



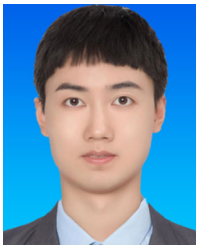
Jintao Meng (Graduate Student Member, IEEE) received the master's degree in control engineering from Anhui University of Science and Technology, Huainan, China, in 2019. He is currently pursuing the Ph.D. degree with ShanghaiTech University, Shanghai, China.

His research interests include energy harvesting, integrated circuit design, smart sensing, and battery-free IoT.



Jiacong Qiu (Graduate Student Member, IEEE) received the B.E. degree in electrical engineering from ShanghaiTech University, Shanghai, China, in 2020, where he is currently pursuing the Ph.D. degree.

His current research interests include energy harvesting and power electronics.



Yilin Wang (Student Member, IEEE) received the B.E. degree in electrical engineering from Shanghai Ocean University, Shanghai, China, in 2022. He is currently pursuing the Ph.D. degree with ShanghaiTech University, Shanghai.

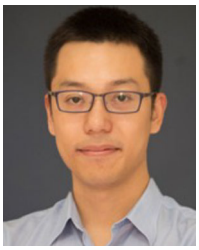
His current research interests include energy harvesting, battery-free Internet of Things, and embedded systems.



Minfan Fu (Senior Member, IEEE) received the B.S., M.S., and Ph.D. degrees in electrical and computer engineering from the University of Michigan Shanghai Jiao Tong University Joint Institute, Shanghai Jiao Tong University, Shanghai, China, in 2010, 2013, and 2016, respectively.

He is a tenured Associate Professor with the School of Information Science and Technology, ShanghaiTech University, Shanghai. His research interests include megahertz wireless power transfer, high-frequency power conversion, high-frequency magnetic design, and the application of wide bandgap devices.

Dr. Fu is currently an Associate Editor of IEEE IES Industrial Electronics Technology News and the Section Chair of several conferences, such as IECON, IPEMC, and VEH. His conference paper for IECON 2019 won the IES-SYPA Competition. He is the Tutorial Speaker for IPEMC 2020 and ISIE 2020.



Haoyu Wang (Senior Member, IEEE) received the bachelor's degree (with Distinguished Hons.) in electrical engineering from Zhejiang University, Hangzhou, China, in 2009, and the Ph.D. degree in electrical engineering from the University of Maryland at College Park, College Park, MD, USA, in 2014.

In 2014, he joined the School of Information Science and Technology, ShanghaiTech University, Shanghai, China, where he is currently a Professor. His research interests include power electronics, plug-in electric and hybrid electric vehicles, the applications of wide bandgap semiconductors, renewable energy harvesting, and power management integrated circuits.

Dr. Wang is a fellow of the Institution of Engineering and Technology (IET). He is an Associate Editor of IEEE TRANSACTIONS ON INDUSTRIAL ELECTRONICS, IEEE TRANSACTIONS ON TRANSPORTATION ELECTRIFICATION, and *CPSS Transactions on Power Electronics and Applications*.



Junrui Liang (Senior Member, IEEE) received the B.E. and M.E. degrees in instrumentation engineering from Shanghai Jiao Tong University, Shanghai, China, in 2004 and 2007, respectively, and the Ph.D. degree in mechanical and automation engineering from The Chinese University of Hong Kong, Hong Kong, China, in 2010.

He is a tenured Associate Professor at the School of Information Science and Technology, ShanghaiTech University, Shanghai. His research interests include energy conversion and power conditioning circuits, kinetic energy harvesting and vibration suppression, IoT devices, and mechatronics.

Dr. Liang is a Fellow of the American Society of Mechanical Engineers (ASME). He is now an Associate Editor of the *Journal of Intelligent Material Systems and Structures* and IEEE CASS NEWSLETTER. He is an IEEE CASS Distinguished Lecturer (2025–2026).

Authorized licensed use limited to: ShanghaiTech University. Downloaded on November 09,2026 at 03:10:32 UTC from IEEE Xplore. Restrictions apply.